IEEE Access
Multidisciplinary ⋮ Rapid Review ⋮ Open Access Journal

Received 15 December 2022, accepted 7 January 2023, date of publication 16 January 2023, date of current version 20 January 2023.

Digital Object Identifier 10.1109/ACCESS.2023.3237396

RESEARCH ARTICLE

Energy Detection for *M*-QAM Signals

SHUN ISHIHARA[1], KENTA UMEBAYASHI[2], (Member, IEEE), AND JANNE J. LEHTOMÄKI[3], (Member, IEEE)

[1]Faculty of Engineering, Tokyo University of Agriculture and Technology, Koganei 184-8588, Japan
[2]Graduate School of Engineering, Tokyo University of Agriculture and Technology, Koganei 184-8588, Japan
[3]Centre for Wireless Communications, University of Oulu, 90014 Oulu, Finland

Corresponding author: Shun Ishihara (ishihara1405@st.go.tuat.ac.jp)

The work of Kenta Umebayashi was supported in part by the European Commission in the Framework of the Project 5GEnhance under Grant H2020-EUJ-02-2018 and Grant 815056, in part by the "Strategic Information and Communications Research and Development Promotion Programme (SCOPE)" of Ministry of Internal Affairs and Communications (MIC) of Japan under Grant JPJ000595, and in part by the Japan Society for the Promotion of Science (JSPS) KAKENHI under Grant JP18KK0109. The work of Janne J. Lehtomäki was supported by the Academy of Finland 6Genesis Flagship under Grant 318927.

ABSTRACT Accurate threshold setting for energy detector is important for example in dynamic spectrum access. This requires accurate statistical distribution models of the observed energy. In this paper, we consider energy detection (ED) for M-ary quadrature amplitude modulation (QAM) signals. The derivation of the exact solution of the distribution model (ES) requires all combinations of QAM signals in the observed signals based on the brute-force search and it leads to a significant computational cost. For this issue, this paper proposes three statistical distribution models which assume $M = \infty$ to avoid the brute-force search. Due to the assumption of M, the proposed models are independent of M and can handle adaptive modulation where M can be changed dynamically. In the numerical evaluations, we compare the three proposed models with the other typical approximation models under additive white Gaussian noise (AWGN) channel and Rayleigh fading channel. In addition, the proposed models are extended for more realistic scenario where imperfect synchronization is considered. The comprehensive numerical evaluations show that the first proposed model is most accurate among all considered models except ES but requires relatively high computational cost. The second proposed model where the observed energy is assumed to follow Gaussian distribution is the least complexity but can have reduced accuracy. The third proposed model based on skew-normal distribution can achieve comparable accuracy and less complexity compared to the first model.

INDEX TERMS Energy detection, quadrature amplitude modulation signal, spectrum sensing, dynamic spectrum access.

I. INTRODUCTION

The rapid increase in wireless communication services had led to the scarcity of spectrum resource and this is currently a significant problem in the wireless communication field. The spectrum resource is usually allocated to each wireless service/system exclusively and new wireless services/systems have difficulty in getting their own spectrum resource since the spectrum is a finite resource [1], [2]. However, according to numerous spectrum usage measurement campaigns, e.g. [3], utilization ratio of the allocated spectrum resource is not always high and may rather be significantly low. This fact indicates that the allocated spectrum resource has not been utilized efficiently.

In order to solve the spectrum scarcity problem, the concept of dynamic spectrum access (DSA) and smart spectrum access have emerged [4], [5], [6]. In the DSA concept, the secondary users (SUs) who do not have own spectrum, can access the unused spectrum owned by licensed users, such as primary users (PUs) and incumbent users, provided that the spectrum usage by the SUs does not cause any harmful interference to PU. One way for the DSA to work is that SUs find spectrum which PU is currently not using. One possible way to find the unused spectrum is spectrum sensing

The associate editor coordinating the review of this manuscript and approving it for publication was Chengpeng Hao.

which can detect whether the spectrum is used by PUs or not [7], [8]. Energy detection (ED), which is one of the spectrum sensing techniques, has several advantages as follows. ED is low complexity in terms of operation and implementation and it does not need a prior information about the received signal [9], [10] unlike other approaches such as the matched filter based spectrum sensing [11], [12].

Consequently, a variety of ED based spectrum sensing approaches have been developed nowadays. In [13], intelligent reflecting surface is used to enhance the performance of spectrum sensing. ED with multiple antenna is analyzed by considering the correlation among antennas [14]. A practical ED scheme has been proposed to detect the presence of a burst signal in [15]. ED with dynamic threshold based on noise measurement is investigated in [16].

The ED used by SU compares observed energy with the predetermined detection threshold. If the observed energy exceeds the threshold, SU decides the spectrum is occupied. Otherwise SU decides the spectrum is idle. Therefore, it is a critical requirement to set a proper detection threshold to achieve the target performance of ED. The detection threshold can be set by the statistical distribution model of observed energy which consists of a possible signal component and a noise component which always exists. Typically, the noise component is assumed to follow a Gaussian distribution and the observed energy with the noise component follows the central Chi-square distribution [17]. On the other hand, the transmitted energy which consists of only signal component can belong to two categories: a deterministic signal and a random signal. In case of constant envelope modulation signal, such as M-ary phase shift keying (PSK) modulation using single carrier technique, the transmitted energy with the signal component can be approximated by a constant value that corresponds to the deterministic signal. In this case, the observed energy follows the non-central Chi-square distribution in additive white Gaussian noise (AWGN) channel [18]. Furthermore, ED for deterministic signals under Rayleigh and Nakagami fading channels was investigated in [19]. In case of random signal, Gaussian approximation for the signal component can provide analytical distributions of the observed energy [17]. For example, the orthogonal frequency division multiplexing (OFDM) signal can be modeled using the Gaussian approximation due to the central limit theorem [20]. Moreover, several works in the literature have approximated the observed energy to a Gaussian distribution under AWGN channel when the number of samples is sufficiently large [21], [22], [23], [24].

The transmitted energy with a quadrature amplitude modulation (QAM) signal based on single carrier technique (such as IEEE standard 802.15.3d-2017 [25]) also belongs to the random signal. Nowadays QAM is attractive because it can achieve the high data rate. In fact, QAM with single carrier communications are investigated for future wireless communications [26], [27], [28]. For the statistical distribution for the observed energy, Gaussian approximation could be one of the options [17], however it dose not always provide an accurate distribution. To tackle this issue, the analysis of ED for the QAM signal (i.e. detection probability) has been investigated in [29]. The analysis can provide an exact solution, called ES in this paper, but it requires enormous computational complexity when the number of samples for ED (K) and modulation order (M) are relatively large. To simplify the derivation, reference [30] has developed an approximation for the observed energy to Gaussian distribution for M-QAM signals. In our preliminary conference paper [31], we proposed a model, called PM1, to obtain the approximated distribution of the observed energy for the QAM signal case under AWGN channel. Instead of the Gaussian approximation, finite M is approximated by infinity to obtain the distribution analytically in PM1. The numerical evaluations in [31] indicated that the accuracy of PM1 is better than the Gaussian approximation of the signal component [17]. PM1 can achieve less computational cost compared to ES in [29]. However, PM1 still requires K-fold convolution and its computational cost is not negligible.

In this paper, we investigate the appropriate statistical models for ED with single carrier based M-QAM signals. The contributions of this paper are summarized as follows.

- In addition to PM1 [31], we propose two further models, defined as PM2 and PM3 in this paper, for the distribution of observed energy in the case of the QAM signal. One of the benefits of the proposed models is that they are independent of M and this is a preferred aspect for adaptive modulation schemes [32] with M-QAM signals. In addition, the proposed models can achieve less complexity compared to the ES [29].
- In PM2, the observed energy is approximated by Gaussian distribution. On the other hand, the transmitted energy of PM3 is approximated by skew normal distribution. PM3 has an advantage in terms of accuracy, while PM2 can achieve relatively lower complexity.
- We investigate the proposed models not only under AWGN channel but also under Rayleigh fading channel. In addition, we also consider the effect of imperfect synchronization in which there is a timing offset in the symbol sampling and it causes intersymbol interference (ISI). Specifically, the proposed model is extended by assuming that ISI component follows Gaussian random process.
- Comprehensive numerical evaluations show the benefits of the proposed models in terms of accuracy as compared to approximated statistical distributions used in the literature ([17], [21], [22], [23], [24], [30]) and in terms of complexity as compared to ES in [29].

The remainder of this paper is organized as follows. First, Section II summarizes energy detection problem considered in this paper. Section III describes statistical distribution models for the observed energy. Specifically, conventional models and three proposed models in cases of AWGN channel and Rayleigh fading channel are shown. In Section IV, comprehensive numerical evaluations based on computer simulations are provided to verify the validity of the proposed models by

their accuracy. Section V summarizes the comparison among the conventional and proposed models based on the numerical evaluations in Section IV. Finally, Section VI concludes this paper.

II. ENERGY DETECTION MODEL

A detection problem in the spectrum sensing can be expressed by a binary hypothesis testing problem in which two hypotheses are $\mathcal{H}_0$ (only noise component) and $\mathcal{H}_1$ (noise and signal components) as [22]:

$$\begin{aligned} \mathcal{H}_0 &: y[k] = w[k] \\ \mathcal{H}_1 &: y[k] = h\sqrt{P}\hat{h}(\tau T)x[k] + I[k] + w[k] \end{aligned} \tag{1}$$

where k ($k = 0, 1, 2, \ldots, K-1$) is the index number for the time domain sample, K is the number of samples during the observation interval for spectrum sensing, $y[k]$ is the kth observed signal at the SU, $\hat{h}(\tau T)$ is an real-valued impulse response of a band limited filter where τ ($-0.5 \leq \tau \leq 0.5$) is timing offset normalized by symbol time duration and T denotes sampling time duration and the symbol time duration, $I[k]$ is ISI component caused by the sampling timing, and $w[k]$ is noise component which follows circularly symmetric complex Gaussian distribution with zero mean and variance σ_n^2. $x[k]$ is a signal component sent from the PU with unit variance, h is the channel gain and P indicates the average power for the signal component.

In this paper, we consider two cases in terms of symbol synchronization as the perfect synchronization case and the imperfect synchronization case. In the perfect synchronization case, the sampled signal is assumed to be able to avoid ISI and it leads to $I[k] = 0$. In the imperfect synchronization case, the ISI component at the k-th sample is given by

$$I[k] = \sqrt{P}\sum_{n\neq 0}\hat{h}((n+\tau)T)x[n+k]. \tag{2}$$

In (1), the noise component is uncorrelated with $x[k]$ and $I[k]$. In this paper, we consider AWGN channel in which $h = 1$ and Rayleigh fading channel in which h follows complex circularly symmetric Gaussian distribution with zero mean and unit variance. Under Rayleigh fading channel, a block fading is assumed and h is constant during one observation interval for spectrum sensing. The average signal to noise power ratio (SNR) and instantaneous SNR are defined by $\gamma = P\hat{h}(0)^2/\sigma_n^2$ and $|h|^2P\hat{h}(0)^2/\sigma_n^2$, respectively. The maximum amplitude of an impulse response is equivalent to $\hat{h}(0)$ and let $\hat{h}(0)$ be unity without loss of generality.

The normalized observed energy V' at the SU is given by:

$$V' = \sum_{k=0}^{K-1}\left(\frac{|y[k]|}{\sqrt{\sigma_n^2/2}}\right)^2 \tag{3}$$

The observed energy is normalized by $\sigma_n^2/2$ in (3) without loss of generality [29]. The assumed modulation type for $x[k]$ is M-ary QAM where M is power of four, such as 16, 64 and 256. The QAM signal provides additional randomness in the observed energy unlike a constant envelope modulation type, such as quadrature phase shift keying (QPSK).

The detection rule in ED is as follows: if V' is larger than the predetermined threshold V_T', the detection result is $\mathcal{H}_1$, otherwise the detection result is $\mathcal{H}_0$, i.e.

$$V' \underset{\mathcal{H}_0}{\overset{\mathcal{H}_1}{\gtrless}} V_T'. \tag{4}$$

The false alarm probability (P_{FA}) and the detection probability (P_D) are used as two criteria to evaluate ED. The event for P_{FA} is that the detection result is $\mathcal{H}_1$ when $\mathcal{H}_0$ is correct hypothesis and the event for P_D is that the detection result is $\mathcal{H}_1$ when $\mathcal{H}_1$ is the correct hypothesis. Mathematically P_{FA} and P_D are given by:

$$P_{FA} = Pr(V' \geq V_T'|\mathcal{H}_0) \tag{5}$$

$$P_D = Pr(V' \geq V_T'|\mathcal{H}_1), \tag{6}$$

where $Pr()$ is the probability of its argument.

III. STATISTICAL DISTRIBUTION MODEL FOR OBSERVED ENERGY

For a proper design of ED, the threshold V_T' is typically set to satisfy either target P_{FA} or target P_D. The normalized observed energy V' under $\mathcal{H}_0$ is given by

$$V' = \sum_{k=0}^{K-1}\left(\frac{w_I[k]}{\sqrt{\sigma_n^2/2}}\right)^2 + \sum_{k=0}^{K-1}\left(\frac{w_Q[k]}{\sqrt{\sigma_n^2/2}}\right)^2. \tag{7}$$

where I and Q indicate inphase and quadrature component, i.e. $x[k] = x_I[k] + jx_Q[k]$, $w[k] = w_I[k] + jw_Q[k]$, $h = h_I + jh_Q$ and $I[k] = I_I[k] + I_Q[k]$. It is well known that the probability density function (PDF) of V' under $\mathcal{H}_0$ follows a central chi-square distribution with $2K$ degrees of freedom (DOF) [18]. The distribution is given by

$$p(V'|\mathcal{H}_0) = p_{\chi^2,2K}(V') = \begin{cases} \dfrac{V'^{K-1}e^{-\frac{V'}{2}}}{2^K\Gamma(K)} & V' > 0 \\ 0 & \text{otherwise} \end{cases} \tag{8}$$

where $\Gamma(K)$ is the gamma function.

On the other hand, P_D depends on the distribution of V' under $\mathcal{H}_1$. In this paper, we focus on the distribution of V' under $\mathcal{H}_1$ since P_D is a critical evaluation criterion in DSA to avoid significant interference.

In this paper, we will show models for the distribution of V' comprehensively. Specifically, ES [29], three conventional Gaussian approximations (CGA) [21], [22], [23], [30], [33], and three proposed models (PM) under three following cases: AWGN channel with perfect synchronization, Rayleigh fading channel with perfect synchronization, and AWGN channel with imperfect synchronization.

A. AWGN CHANNEL WITH PERFECT SYNCHRONIZATION

In the AWGN with perfect synchronization case, $h = 1$ and $I[k] = 0$ due to no ISI in (1). Let λ_A denote the normalized

observed energy due to the signal component in V'. V' and λ_A are expressed by

$$2V' = \sum_{k=0}^{K-1}\left(\frac{\sqrt{P}x_I[k]+w_I[k]}{\sqrt{\sigma_n^2/2}}\right)^2 + \sum_{k=0}^{K-1}\left(\frac{\sqrt{P}x_Q[k]+w_Q[k]}{\sqrt{\sigma_n^2/2}}\right)^2, \quad (9)$$

and,

$$\lambda_A = \sum_{k=0}^{K-1}\left(\frac{\sqrt{P}x_I[k]}{\sqrt{\sigma_n^2/2}}\right)^2 + \sum_{k=0}^{K-1}\left(\frac{\sqrt{P}x_Q[k]}{\sqrt{\sigma_n^2/2}}\right)^2, \quad (10)$$

respectively. For a given λ_A, PDF of V' under $\mathcal{H}_1$ follows a noncentral chi-square distribution with $2K$ DOF as

$$p(V'|\lambda_A,\mathcal{H}_1) = p_{\chi^2,2K}(V'|\lambda_A) = \sum_{i=0}^{\infty}\frac{e^{\frac{-\lambda_A}{2}}(\frac{-\lambda_A}{2})^i}{i!}p_{\chi^2,2K+2i}(V'), \quad (11)$$

and λ_A is known as the non-centrality parameter in the chi-square distribution [17]. In this case, an achievable P_D with given threshold V_T' and λ_A is [29]:

$$P_D(V_T'|\lambda_A) = Q_K\left(\sqrt{\lambda_A},\sqrt{V_T'}\right), \quad (12)$$

where $Q_K(\cdot)$ is the generalized Marcum Q-function [34].

In case of QAM, λ_A is random and let $p_A(\lambda_A)$ denote the distribution of λ_A. In this case, PDF of $p(V'|\mathcal{H}_1)$ is given by

$$p(V'|\mathcal{H}_1) = \int_0^\infty p_{\chi^2,2K}(V'|\lambda_A)p_A(\lambda_A)d\lambda_A. \quad (13)$$

Similarly, by averaging (12) over $p_A(\lambda_A)$, average P_D can be obtained by [35]

$$\begin{aligned}P_D(V_T') &= \int_{V_T'}^\infty p(V'|\mathcal{H}_1)dV' \\ &= \int_0^\infty P_D(V_T'|\lambda_A)p_A(\lambda_A)d\lambda_A \\ &= \int_0^\infty Q_K\left(\sqrt{\lambda_A},\sqrt{V_T'}\right)p_A(\lambda_A)d\lambda_A. \end{aligned} \quad (14)$$

The equations in (13) and (14) indicate that either $p_A(\lambda_A)$ or $p(V'|\mathcal{H}_1)$ is necessary to set the threshold to satisfy the target P_D.

1) EXACT SOLUTION (ES)

In [29], a model to obtain the distribution of observed energy due to signal component, λ_A, was shown. Let $\mathbb{E_S}^K$ denote the sample space of observed energy contributed by signal component during K samples. Thus, the exact $p_A(\lambda_A)$ can be expressed by

$$p_A(\lambda_A) = \sum_{\epsilon\in\mathbb{E_S}^K}\delta(\lambda_A-\epsilon)Pr(\epsilon), \quad (15)$$

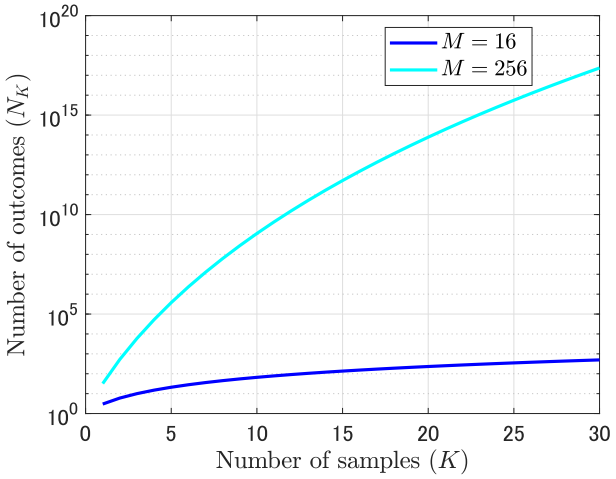

FIGURE 1. The number of outcomes as a function of the number of samples.

where $Pr(\epsilon)$ denotes probability of observed energy ϵ due to the signal components. Then, by using (14), P_D is given by

$$P_D(V_T'|\lambda_A) = \sum_{\epsilon\in\mathbb{E_S}^K}Pr(\epsilon)Q_K(\sqrt{\lambda_A(\epsilon)},\sqrt{V_T'}). \quad (16)$$

One issue in this model is that the number of elements in the set $\mathbb{E_S}^K$ can be significantly large. For instance, the number of elements in $\mathbb{E_S}^K$ is denoted by N_K which is given by [29]:

$$N_K = \frac{(N_1+K-1)!}{(N_1-1)!K!}, \quad (17)$$

where N_1 indicates possible energy levels for M-QAM. In case of 16-QAM, $N_1 = 3$.

In Fig. 1, N_K as a function of K for $M = 16$ and $M = 256$ are plotted. For larger M, such as $M = 256$, N_K increases significantly as K increases. In fact, K can be more than 100 samples and this leads to significantly large N_K.

2) CONVENTIONAL GAUSSIAN APPROXIMATIONS (CGAs)

Three CGA based models to obtain approximated distribution of V' are shown in this section. In the first CGA (CGA1), $x[k]$ is assumed to follow Gaussian distribution since the signal component is random process due to QAM. In this case $p(V'|H_1)$ follows the generalized chi-squared distribution [33]:

$$p(V'|\mathcal{H}_1) = \begin{cases}\dfrac{V'^{K-1}e^{-\frac{V'}{2(1+\gamma)}}}{(2(1+\gamma))^K\Gamma(K)} & V'>0 \\ 0 & \text{otherwise.}\end{cases} \quad (18)$$

In the second CGA (CGA2), not only $x[k]$, but also V' are assumed to follow Gaussian distribution as [21], [22], [23]:

$$V' \sim \mathcal{N}\left(2K(\gamma+1), 4K(\gamma+1)^2\right). \quad (19)$$

This approximation is valid when K is large number due to the central limit theorem.

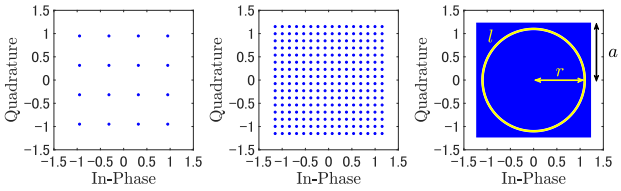

(a) $M = 16$ (b) $M = 256$ (c) $M = \infty$

FIGURE 2. Constellation points for M-QAM.

In the third CGA (CGA3), V' is approximated by Gaussian distribution while $x[k]$ is the M-QAM signal as [30]:

$$V' \sim \mathcal{N}\left(2K(\gamma+1), 4K\left(\frac{2}{5}\frac{M-4}{M-1}\gamma^2+2\gamma+1\right)\right), \tag{20}$$

in which the mean and variance have been obtained based on exact statistics of M-QAM signals.

3) PROPOSED MODELS (PMs)

In the three proposed models (PM1, PM2 and PM3), $p_A(\lambda_A)$ is approximated by assuming $M = \infty$. In Fig. 2, constellation points for different M (16, 256, and ∞) in QAM signals are plotted. This figure indicates that the distributions of $x[k]$ have a square shape. According to this fact, the PDF of λ_A with $K = 1$ and $M = \infty$ under AWGN channel can be expressed by

$$p_{\infty,1,A}(\lambda_A) = \begin{cases} \dfrac{\pi}{8\gamma a^2} & (0 < \lambda_A \le 2\gamma a^2) \\ \dfrac{\frac{\pi}{2} - 2\cos^{-1}\sqrt{\frac{2\gamma a^2}{\lambda_A}}}{4\gamma a^2} & (2\gamma a^2 \le \lambda_A \le 4\gamma a^2), \end{cases} \tag{21}$$

where suffix 1 of $p_{\infty,1,A}(\lambda_A)$ indicates that $K = 1$. The details of the derivation of $p_{\infty,1,A}(\lambda_A)$ are shown in Appendix A. For the general K, $p_{\infty,K,A}(\lambda_A)$ can be obtained by

$$p_{\infty,K,A}(\lambda_A) = \overbrace{p_{\infty,1,A}(\lambda_A) * p_{\infty,1,A}(\lambda_A) \cdots p_{\infty,1,A}(\lambda_A)}^{K}, \tag{22}$$

where $*$ denotes convolution. It has been well known that the complexity of the convolution can be reduced from quadratic computational complexity to linearithmic computational complexity by employing fast Fourier transform [36]. The approximated $p(V'|\mathcal{H}_1)$ can be obtained by plugging in $p_{\infty,K,A}(\lambda_A)$ for (13). This distribution $p(V'|\mathcal{H}_1)$ is denoted by PM1.

In the second proposed model (PM2), the Gaussian approximation is applied for PM1. Specifically, $p(V'|\mathcal{H}_1)$ in PM2 is approximated to be Gaussian distribution with mean $\mu_{V'}$ and variance $\sigma^2_{V'}$. For a given λ_A, V' follows the non-central chi-squared distribution with the mean and variance given by

$$\mu_{V'|\lambda_A} = 2K + \lambda_A$$
$$\sigma^2_{V'|\lambda_A} = 4K + 4\lambda_A.$$

Next, mean and variance of λ_A are given by

$$\mu_{\lambda_A} = 2K\gamma \tag{23}$$
$$\sigma^2_{\lambda_A} = \frac{8}{5}K\gamma^2, \tag{24}$$

and the details of the derivation of μ_{λ_A} and $\sigma^2_{\lambda_A}$ are shown in Appendix B. According to the law of total expectation and law of total variance [37], $\mu_{V'}$ and $\sigma^2_{V'}$ are given by

$$\mu_{V'} = 2K\gamma + 2K \tag{25}$$
$$\sigma^2_{V'} = \frac{8}{5}K\gamma^2 + 8K\gamma + 4K. \tag{26}$$

Therefore, the distribution of V' in PM2 is given by

$$V' \sim \mathcal{N}\left(2K(\gamma+1), 4K\left(\frac{2}{5}\gamma^2+2\gamma+1\right)\right). \tag{27}$$

PM2 has a significant benefit in terms of computational complexity compared to PM1.

In PM1, the integration calculations in (22) is not negligible especially when K is large even if FFT is employed. For this issue, PM3 uses skew normal distribution [38] with parameters ξ, ω and α to approximate (22). The distribution approximated by skew normal distribution $p_s(\lambda_A)$ is expressed by

$$p_s(\lambda_A) = \frac{2}{\omega}\phi\left(\frac{\lambda_A-\xi}{\omega}\right)\Phi\left(\alpha\left(\frac{\lambda_A-\xi}{\omega}\right)\right) \tag{28}$$

where $\phi(x)$ and $\Phi(x)$ are Gaussian probability density function and Gaussian cumulative distribution function, given by

$$\phi(x) = \frac{1}{\sqrt{2\pi}}e^{-\frac{x^2}{2}}, \tag{29}$$
$$\Phi(x) = \int_{-\infty}^{x}\frac{1}{\sqrt{2\pi}}e^{-\frac{t^2}{2}}dt, \tag{30}$$

respectively. The parameters α, ω and ξ are given by mean μ_{λ_A} and variance $\sigma^2_{\lambda_A}$ as follows:

$$\alpha = \frac{\delta}{\sqrt{|1-\delta^2|}}, \tag{31}$$
$$\omega = \sqrt{\frac{\sigma^2_{\lambda_A}}{1-\frac{2\delta^2}{\pi}}}, \tag{32}$$
$$\xi = \mu_{\lambda_A} - \omega\delta\sqrt{\frac{2}{\pi}}, \tag{33}$$

where δ is

$$\delta = \frac{\kappa_{\lambda_A}}{|\kappa_{\lambda_A}|}\sqrt{\frac{\pi}{2}\frac{|\kappa_{\lambda_A}|^{\frac{2}{3}}}{\left(\frac{4-\pi}{2}\right)^{\frac{2}{3}}+|\kappa_{\lambda_A}|^{\frac{2}{3}}}}, \tag{34}$$

where κ_{λ_A} is skewness of λ_A and given by

$$\kappa_{\lambda_A} = \frac{\sqrt{10}}{7\sqrt{K}}. \tag{35}$$

The details of derivation in terms of skewness κ_{λ_A} is shown in Appendix B.

B. RAYLEIGH FADING CHANNEL WITH PERFECT SYNCHRONIZATION

In case of Rayleigh fading channel, the models can be categorized into two types. In the first type, the distribution of signal component λ_A under AWGN channel is used and this corresponds to CGA1, PM1, and PM3. In the second type, the Gaussian approximation is applied for the observed energy under AWGN channel and this corresponds to CGA2, CGA3 and PM2. The distributions of the signal component under AWGN channel and Rayleigh fading channel are denoted by $p_A(\lambda_A)$ and $p_F(\lambda_F)$, respectively.

1) CGA1, PM1, AND PM3

Under Rayleigh fading channel, h follows complex circularly symmetric Gaussian distribution with zero mean and unit variance. In this case, the normalized observed energy V' is given by

$$V' = \sum_{k=0}^{K-1}\left(\frac{\sqrt{P}\left(h_I x_I[k] - h_Q x_Q[k]\right) + w_I[k]}{\sqrt{\sigma_n^2/2}}\right)^2 + \sum_{k=0}^{K-1}\left(\frac{\sqrt{P}\left(h_Q x_I[k] + h_I x_Q[k]\right) + w_Q[k]}{\sqrt{\sigma_n^2/2}}\right)^2 \tag{36}$$

Besides, the normalized transmitted energy of signal component after a fading channel, λ_F, is given by

$$\begin{aligned}\lambda_F &= \sum_{k=0}^{K-1}\left(\frac{|h|\sqrt{P}x_I[k]}{\sqrt{\sigma_n^2/2}}\right)^2 + \sum_{k=0}^{K-1}\left(\frac{|h|\sqrt{P}x_Q[k]}{\sqrt{\sigma_n^2/2}}\right)^2 \\ &= |h|^2\left\{\sum_{k=0}^{K-1}\left(\frac{\sqrt{P}x_I[k]}{\sqrt{\sigma_n^2/2}}\right)^2 + \sum_{k=0}^{K-1}\left(\frac{\sqrt{P}x_Q[k]}{\sqrt{\sigma_n^2/2}}\right)^2\right\} \\ &= |h|^2\lambda_A. \end{aligned} \tag{37}$$

For a given $p_A(\lambda_A)$, $p_F(\lambda_F)$ is given by

$$p_F(\lambda_F) = \int_0^\infty\int_0^\infty \delta\left(\lambda_F - |h|^2\lambda_A\right) p_A(\lambda_A) \cdot \exp(-|h|^2) d|h|^2 d\lambda_A, \tag{38}$$

where

$$\delta(x) = \begin{cases}\infty, & x = 0 \\ 0, & x \neq 0\end{cases}$$

is Dirac delta function, and $|h|^2$ follows exponential distribution as $p(|h|^2) = \exp(-|h|^2)$ under Rayleigh fading channel.

Based on (13) and (38), $p(V'|\mathcal{H}_1)$ under Rayleigh fading channel can be calculated as follows:

$$\begin{aligned} &p(V'|\mathcal{H}_1) \\ &= \int_0^\infty p_{\chi^2,2K}(V'|\lambda_F) p_F(\lambda_F) d\lambda_F, \\ &= \int_0^\infty\int_0^\infty\int_0^\infty p_{\chi^2,2K}(V'|\lambda_F)\delta\left(\lambda_F - |h|^2\lambda_A\right) d\lambda_F \\ &\quad \cdot \exp(-|h|^2) d|h|^2 p_A(\lambda_A) d\lambda_A, \\ &= \int_0^\infty\int_0^\infty p_{\chi^2,2K}(V'||h|^2\lambda_A)\exp(-|h|^2) d|h|^2 p_A(\lambda_A) d\lambda_A, \\ &= \int_0^\infty p_{F,2K}(V'|\lambda_A) p_A(\lambda_A) d\lambda_A, \end{aligned} \tag{39}$$

where

$$p_{F,2K}(V'|\lambda_A) = \int_0^\infty p_{\chi^2,2K}(V'||h|^2\lambda_A)\exp(-|h|^2) d|h|^2. \tag{40}$$

$p_{F,2K}(V'|\lambda_A)$ can be interpreted as the distribution of the observed energy with given λ_A under Rayleigh fading channel. According to [39], $p_{F,2K}(V'|\lambda_A)$ is given by

$$CClp_{F,2K}(V'|\lambda_A) = \left(\frac{\lambda_A + 2}{\lambda_A}\right)^{K-1} p_e(V'|\lambda_A + 2) \cdot P\left(K - 1, \frac{\lambda_A V'}{2(\lambda_A + 2)}\right), \tag{41}$$

where $P(a, b) = \gamma(a, b)/\Gamma(a)$ is the normalized incomplete gamma function and $\gamma(a, b)$ is the lower incomplete gamma function. The $p_e(x|a)$ is the exponential probability density function defined as:

$$p_e(x|a) = H(x)\frac{\exp\left(-\frac{x}{a}\right)}{a}, \tag{42}$$

where $H(x) = \begin{cases}1, & x \geq 0 \\ 0, & x < 0\end{cases}$ is the Heaviside step function. In addition, the achievable P_D with given threshold V_T' and λ_A in Rayleigh fading case is [19], [39]:

$$P_D(V_T'|\lambda_A) = e^{-\frac{V_T'}{2}}\sum_{n=0}^{K-2}\frac{1}{n!}\left(\frac{V_T'}{2}\right)^n + \left(\frac{\lambda_A + 2}{\lambda_A}\right)^{K-1} \cdot \left[e^{-\frac{V_T'}{\lambda_A+2}} - e^{-\frac{V_T'}{2}}\sum_{n=0}^{K-2}\frac{1}{n!}\left(\frac{\lambda_A V_T'}{2(\lambda_A + 2)}\right)^n\right]. \tag{43}$$

Finally, P_D under Rayleigh fading channel is given by:

$$\begin{aligned} P_D(V_T') &= \int_{V_T'}^\infty p(V'|\mathcal{H}_1) dV' \\ &= \int_0^\infty P_D(V_T'|\lambda_A) p_A(\lambda_A) d\lambda_A. \end{aligned} \tag{44}$$

(41)-(44) indicate P_D under Rayleigh fading channel also requires $p(V'|\mathcal{H}_1)$ or $p_A(\lambda_A)$.

2) CGA2, CGA3, AND PM2

In the second type, the Gaussian approximation is applied for the observed energy under AWGN channel. Based on (39), $p(V'|\mathcal{H}_1)$ under Rayleigh fading channel can also be expressed as follows:

$$\begin{aligned} &p(V'|\mathcal{H}_1) \\ &= \int_0^\infty \int_0^\infty p_{\chi^2,2K}(V'||h|^2\lambda_A)\exp(-|h|^2)d|h|^2 p_A(\lambda_A)d\lambda_A \\ &= \int_0^\infty \int_0^\infty p_{\chi^2,2K}(V'||h|^2\lambda_A)p_A(\lambda_A)d\lambda_A \exp(-|h|^2)d|h|^2 \\ &= \int_0^\infty p(V'||h|^2,\mathcal{H}_1)\exp(-|h|^2)d|h|^2, \end{aligned} \tag{45}$$

where $p(V'||h|^2,\mathcal{H}_1)$ can be interpreted as the distribution of the observed energy under AWGN channel when a channel gain $|h|^2$ is given. The distribution of V' under the Rayleigh fading is given by the Gaussian approximation of $p(V'||h|^2,\mathcal{H}_1)$:

$$p(V'|\mathcal{H}_1) = \int_0^\infty \phi\left(\frac{V'-\mu_{V'||h|^2}}{\sigma_{V'||h|^2}}\right)\exp(-|h|^2)d|h|^2, \tag{46}$$

where $\mu_{V'||h|^2}$ and $\sigma^2_{V'||h|^2}$ are mean and variance of the approximated Gaussian distribution of V' with a given $|h|^2$, respectively. The mean and variance with given $|h|^2$ depend on each model, such as CGA2, CGA3, and PM2. According to (19), (20), (25) and (26), they are as follows:

$$\begin{aligned} \mu^{CGA2}_{V'||h|^2} &= 2K|h|^2\gamma + 2K, \\ \mu^{PM2}_{V'||h|^2} &= 2K|h|^2\gamma + 2K, \\ \sigma^2{}^{CGA2}_{V'||h|^2} &= 4K(|h|^2\gamma+1)^2, \\ \sigma^2{}^{CGA3}_{V'||h|^2} &= 4K\left(\frac{2}{5}\frac{M-4}{M-1}|h|^4\gamma^2 + 2|h|^2\gamma + 1\right), \\ \sigma^2{}^{PM2}_{V'||h|^2} &= \frac{8}{5}K|h|^4\gamma^2 + 8K|h|^2\gamma + 4K. \end{aligned} \tag{47}$$

C. AWGN CHANNEL WITH IMPERFECT SYNCHRONIZATION

In the imperfect synchronization case, τ is nonzero and it leads to ISI with the interference component $I[k]$. $I[k]$ is the sum of interference signals from the neighboring symbols and thus $I[k]$ can be approximated as Gaussian random variable due to the central limit theorem. The received signal can be approximated by

$$y[k] \simeq \sqrt{P}\hat{h}(\tau T)x[k] + w'[k], \tag{48}$$

where $w'[k] = I[k] + w[k]$ is assumed to follow circularly symmetric complex Gaussian distribution with zero mean and variance $\sigma_n^2 + \sigma_I^2$, where σ_I^2 is the variance of $I[k]$ given by

$$\sigma_I^2 = P\sum_{n\neq 0}\hat{h}((n+\tau)T)^2. \tag{49}$$

The normalized observed energy is also approximated as:

$$V' \simeq \frac{\sigma_n^2+\sigma_I^2}{\sigma_n^2}V'_I, \tag{50}$$

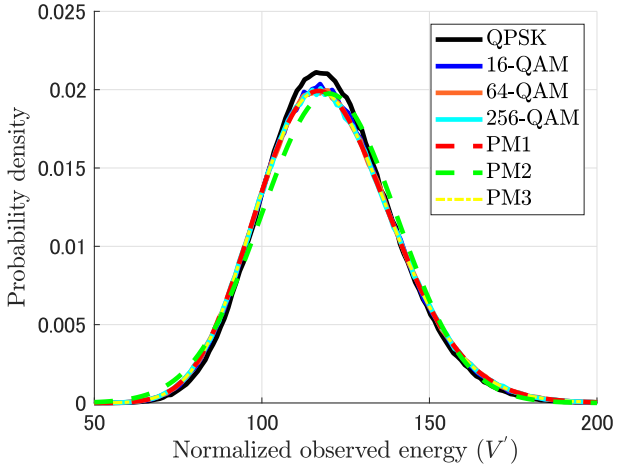

FIGURE 3. PDF of normalized observed energy for empirical distributions and PM1,2,3 with $\gamma = 0$ dB and $K = 30$ under AWGN channel in perfect synchronization case.

where

$$V'_I = \sum_{k=0}^{K-1}\left(\frac{\sqrt{P}\hat{h}(\tau T)x_I[k] + w'_I[k]}{\sqrt{(\sigma_n^2+\sigma_I^2)/2}}\right)^2 + \sum_{k=0}^{K-1}\left(\frac{\sqrt{P}\hat{h}(\tau T)x_Q[k] + w'_Q[k]}{\sqrt{(\sigma_n^2+\sigma_I^2)/2}}\right)^2. \tag{51}$$

As compared to (9), V'_I in (51) can be interpreted as the observed energy in III-A. In this case, signal to noise and interference power ratio (SINR) γ' is given by

$$\gamma' = \frac{P\hat{h}(\tau T)^2}{\sigma_n^2+\sigma_I^2}. \tag{52}$$

In the statistics for PMs of the perfect synchronization case, SNR γ is used in (21)-(26). For the PMs in the imperfect synchronization case, the appropriate PDFs of observed energy are available by replacing γ with γ'.

IV. NUMERICAL EVALUATIONS

For the evaluations of the models (CGA1, CGA2, CGA3, PM1, PM2 and PM3), we employ probability density function (PDF), Kolmogorov-Smirnov (KS) statistics, and detection probability (P_D). PDF of normalized observed energy V' shows the comparison of visual accuracy between empirical distribution and the distributions based on our proposed models. Generally, PDF is used for the ED design. Specifically, based on the accurate PDF and target P_{FA} or P_D, the threshold can be set properly. The KS statistics can indicate the accuracy of the distribution numerically. Finally, P_D can indicate the accuracy of each model in the scenario of spectrum sensing.

A. AWGN CHANNEL WITH PERFECT SYNCHRONIZATION

In Fig. 3, the PDFs of V' by the proposed models (PM1, PM2 and PM3) and empirical PDFs with $M = 4, 16, 64$ and 256 for

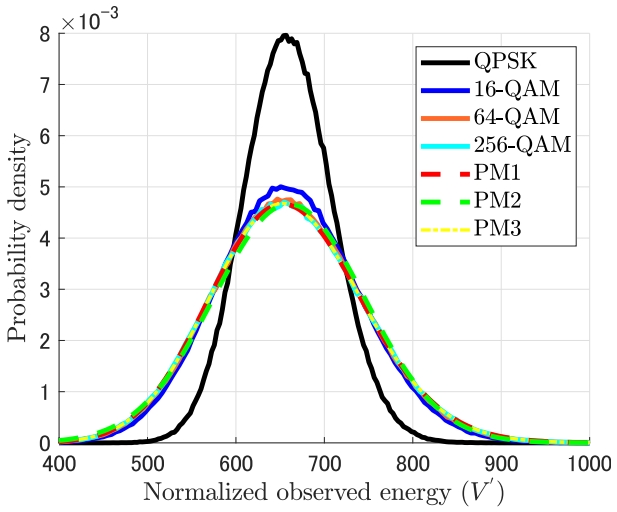

FIGURE 4. PDF of normalized observed energy for empirical distributions and PM1,2,3 with $\gamma = 10$ dB and $K = 30$ under AWGN channel in perfect synchronization case.

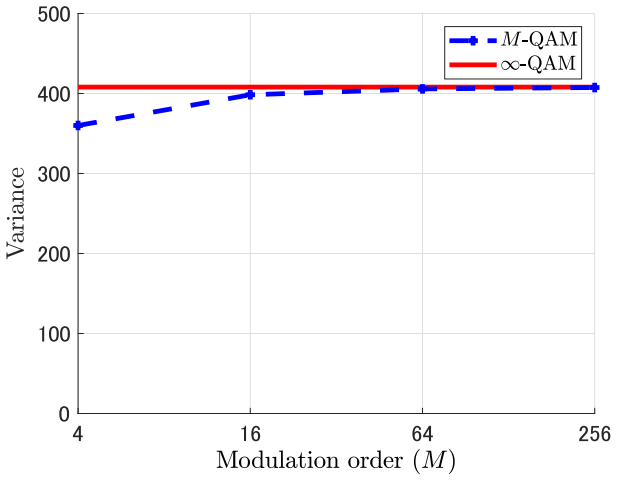

FIGURE 5. The variance of observed energy as a function of M with $K = 30$ and $\gamma = 0$ dB under AWGN channel in perfect synchronization case.

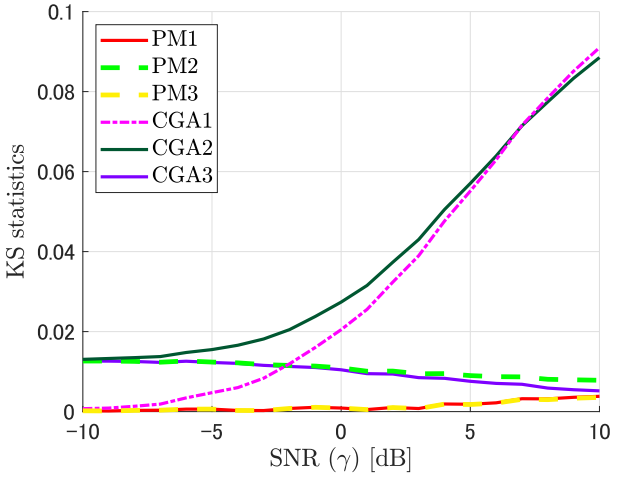

FIGURE 6. KS statistics as a function of γ with $M = 64$ and $K = 30$ under AWGN channel in perfect synchronization case.

$\gamma = 0$ dB and $K = 30$ are plotted. The modulation type with $M = 4$ corresponds to QPSK. Notice that the empirical PDFs with $M \geq 16$ and the distribution with the three proposed models approximately coincide except the empirical distribution with QPSK. In the case of QPSK, λ_A is deterministic since QPSK is a constant envelope modulation while λ_A with $M \geq 16$ is random. In addition, we can confirm the small error between the PDF with PM2 and the empirical PDFs. This result indicates the validity of approximation ($M = \infty$) in the three proposed models.

In Fig. 4, the PDFs of V' in case of high SNR are shown. Specifically, the PDFs of V' by the three proposed models (PM1, PM2 and PM3) and empirical PDFs for $\gamma = 10$ dB and $K = 30$ are plotted. In the relatively high SNR case, the PDFs with the three proposed models still approximately coincide with the empirical PDFs with $M \geq 64$. On the other hand, the empirical PDF with $M = 16$ is slightly different from the other empirical PDFs with $M \geq 64$. The results in Figs. 3 and 4 indicate that the proposed model is relatively more accurate in low SNR. This is the preferred aspect since spectrum sensing in dynamic spectrum access is usually conducted in relatively low SNR such as less than 0 dB [40], [41], [42].

In Figs. 3 and 4, the empirical PDFs as a function of normalized observed energy with larger M get closer to the proposed model distribution. This aspect is more clearly confirmed in Fig. 4 and the statistics of observed energy in (20). The mean of observed energy does not depend on M. In addition, the term $(M-4)/(M-1)$ in the variance component in (20) converges to 1 as M increases. These facts imply that the PDF for larger M converges to one PDF with $M = \infty$. To confirm this aspect, Fig. 5 shows the variance component in (20) against M. The variance of finite M asymptotically approach to the variance of infinite M, while the variances when finite M is small e.g., $M = 16$, can be approximated to the variance when M is infinite. This is the reason why the proposed model which assume $M = \infty$ can provide an accurate PDF.

Now we will evaluate the approximation models by Kolmogorov-Smirnov (KS) statistic [43], [44], [45]. The KS statistics indicates a difference between empirical cumulative distribution function (CDF) $F_{Emp}(V')$ and CDF obtained from the approximation model $F_{Model}(V')$ by

$$D_{KS} = \max_{V'_{KS} < V' < \infty} |F_{Emp}(V') - F_{Model}(V')|, \quad (53)$$

where V'_{KS} is used to determine a range for the CDF. $F_{Emp}(V')$ is obtained by empirical simulation and $F_{Model}(V')$ is given by $1 - P_D(V')$ with (14) for AWGN channel and with (44) under Rayleigh fading channel. Without loss of generality, V'_{KS} is set to satisfy $F_{Emp}(V'_{KS}) = 0.1$. The reason of $F_{Emp}(V'_{KS}) = 0.1$ is to evaluate the KS statistics in the

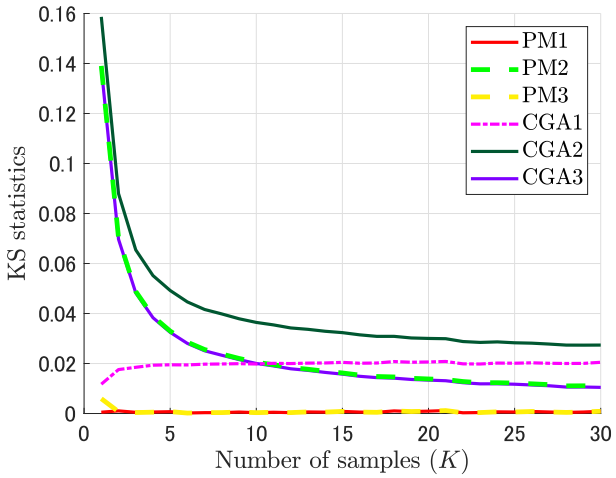

FIGURE 7. KS statistics as a function of K with $M = 64$ and $\gamma = 0$ dB under AWGN channel in perfect synchronization case.

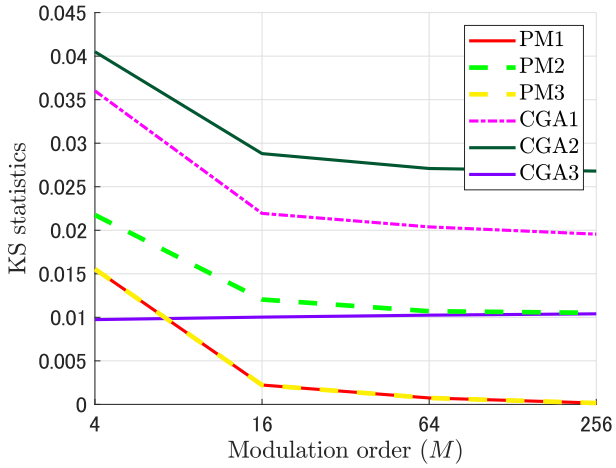

FIGURE 8. KS statistics as a function of M with $K = 30$ and $\gamma = 0$ dB under AWGN channel in perfect synchronization case.

region in terms of CDF where $P_D \geq 0.9$ according to the requirement of P_D in the IEEE 802.22 standard [46].

Fig. 6 shows the KS statistics as a function of SNR (γ) for $M = 64$ and $K = 30$ in the AWGN channel. The accuracy of CGA1 and CGA2 gets significantly worse as SNR increases while other approximation models can achieve relatively accurate performance. This is because both CGA1 and CGA2 assume that the signal component follows Gaussian distribution while the other approximation models consider the actual statistics of the QAM signal. In addition, PM1 and PM3 can achieve the most accurate performance in the considered SNR region.

Fig. 7 shows KS statistics as a function of K (the number of samples) for $M = 64$ and $\gamma = 0$ dB. In the whole K region, PM1 can achieve the best accuracy. PM3 can achieve comparable performance with PM1 except for $K = 1$. In the low K region such as $K < 10$, CGA1 can achieve relatively accurate performance. On the other hand, in the high K region, PM2 and CGA3 can outperform CGA1.

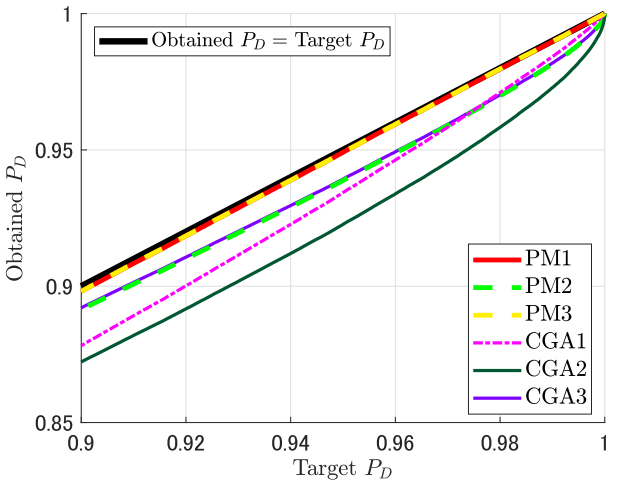

FIGURE 9. Obtained P_D as function of target P_D for $M = 64$ where $K = 30$ and $\gamma = 0$ dB under AWGN channel in perfect synchronization case.

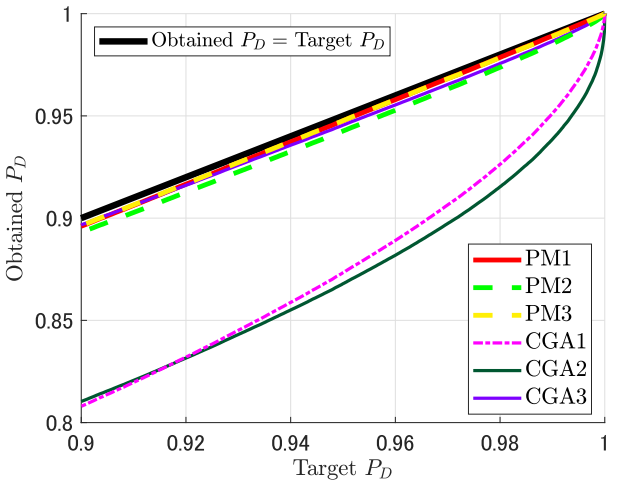

FIGURE 10. Obtained P_D as function of target P_D for $M = 64$ where $K = 30$ and $\gamma = 10$ dB under AWGN channel in perfect synchronization case.

In Fig. 8, the KS statistics as a function of M for $\gamma = 0$ dB and $K = 30$ is shown. The KS performance of CGA3 is independent of M while KS performances of the other approximation models is improved for higher number of M. In most of M, PM1 and PM3 can achieve the best accuracy.

In the following part, we evaluate the effect of accuracy of the approximation models in the spectrum sensing performance. Constant detection rate (CDR) rule is adopted where ED threshold is set to satisfy a target P_D [47]. There would be a gap between the target P_D and obtained P_D due to the approximations in each model.

In Fig. 9, the obtained P_D as a function of target P_D with $\gamma = 0$ dB is shown. This result corresponds to low SNR case. In this evaluation, the target region of P_D is set to more than 0.9 [48]. PM1 and PM3 can achieve the most accurate performance compared to the other models.

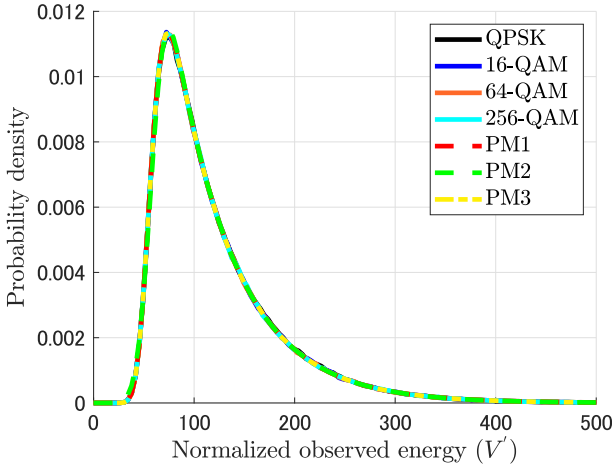

FIGURE 11. PDF of normalized observed energy for empirical distributions and PM1,2,3 with $\gamma = 0$ dB and $K = 30$ under Rayleigh fading channel in perfect synchronization case.

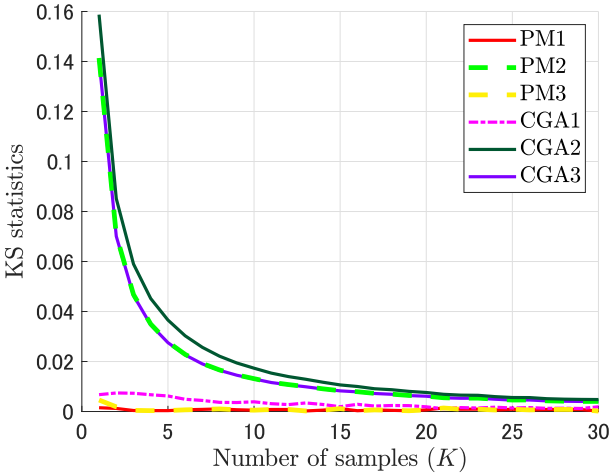

FIGURE 13. KS statistics as a function of K with $M = 64$ and $\gamma = 0$ dB under Rayleigh fading channel in perfect synchronization case.

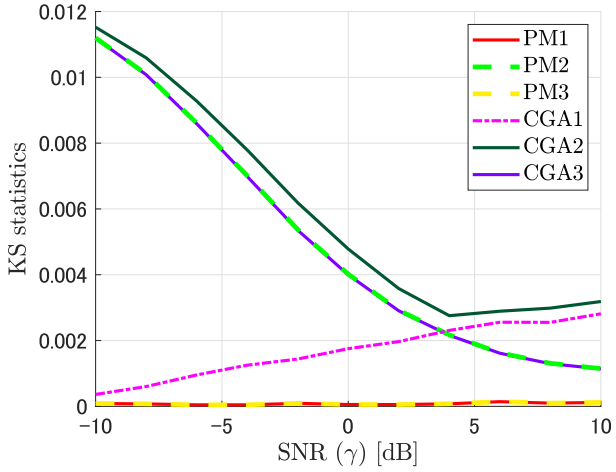

FIGURE 12. KS statistics as a function of γ with $M = 64$ and $K = 30$ under Rayleigh fading channel in perfect synchronization case.

In Fig. 10, the obtained P_D as a function of target P_D with high SNR case $\gamma = 10$ dB is shown. In the high SNR case, not only PM1 and PM3, but also PM2 and CGA3 can achieve almost equivalent performance. However, in CGA1 and CGA2, the gaps between the obtained P_D and the target P_D are increased.

From the results under AWGN channel, PM1 and PM3 can achieve the best performance while the computational cost of PM3 is less than PM1. PM2 and CGA3 can achieve relatively better performance than CGA1 and CGA2 since PM2 and CGA3 consider the characteristics of QAM signal in the approximations.

B. FADING CHANNEL WITH PERFECT SYNCHRONIZATION

In this section, we evaluate the approximation models under Rayleigh fading channel. In Fig. 11, the PDFs of the proposed models and empirical PDFs with $M = 4$, 16, 64 and 256 for $\gamma = 0$ dB is shown. The result indicates that all PDFs approximately coincide. As already shown in Figs. 3 and 4, the PDFs of the observed energy of M-QAM signals can be approximated to the PDF with $M = \infty$. According to (45), the PDF of observed energy under fading channel is equivalent to the expectation of distribution under AWGN channel over realized channel gain $|h|^2$. Therefore, the approximation with $M = \infty$ also works appropriately under the fading channel.

The model based on PM1 can provide accurate distributions for all M and the empirical distributions indicate that M is not significant parameter to determine the shape of distribution. Fig. 12 shows the KS statistics as a function of SNR for $M = 64$ and $K = 30$. The KS performances under Rayleigh fading channel are better than the performances under AWGN channel, such as result in Fig. 6. Under Rayleigh fading channel, PM1 and PM3 can also achieve the most accurate performance in whole SNR region. Unlike the case under AWGN channel, CGA1 can achieve relatively good performance. This is because the signal component under Rayleigh fading channel has not only randomness due to QAM, but also randomness due to the fading channel.

Fig. 13 shows the KS statistics as a function of K for $M = 64$ and $\gamma = 0$ dB. PM1 can again achieve the best performance while PM3 achieve nearly the same performance as PM1 except for $K = 1$. In addition, CGA1 can also achieve relatively accurate performance. On the other hand, PM2 and CGA2 and CGA3 require the large number of K to achieve the accurate performance. This result indicate that the Gaussian approximation for observed energy can be valid for the large number of K.

Fig. 14 shows the KS statistics as a function of M for $K = 30$ and $\gamma = 0$ dB. The result indicates that the KS performance depends much less on M under Rayleigh fading channel than under AWGN channel.

The effects of the model accuracy to the the spectrum sensing performance under CDR rule in fading channel are evaluated in Fig. 15. Specifically, obtained P_D as a function

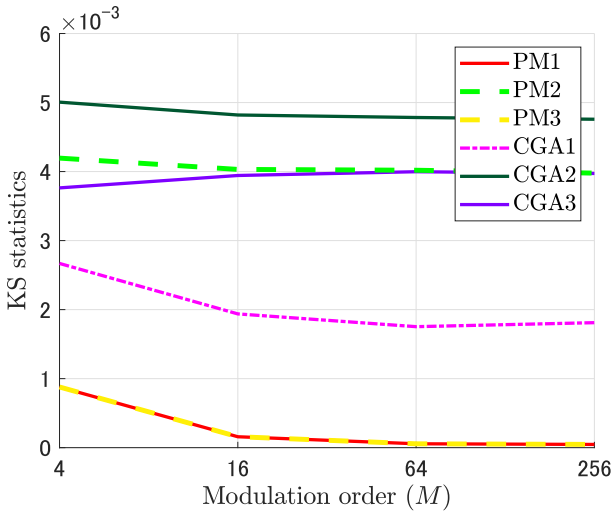

FIGURE 14. KS statistics as a function of M with $K = 30$ and $\gamma = 0$ dB under Rayleigh fading channel in perfect synchronization case.

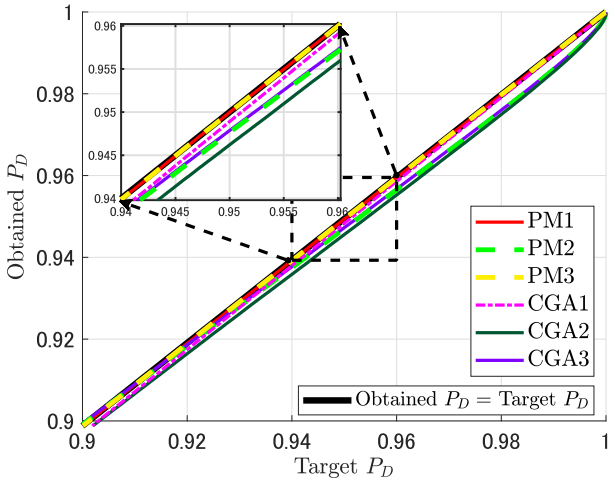

FIGURE 15. Obtained P_D as function of target P_D for $M = 64$ where $K = 30$ and $\gamma = 0$ dB under Rayleigh fading channel in perfect synchronization case.

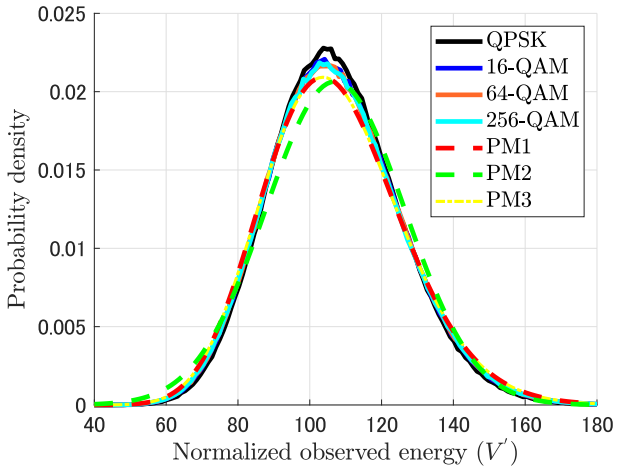

FIGURE 16. PDF of normalized observed energy for empirical distributions and PM1, 2, 3 with $\gamma = 0$ dB, $K = 30$ and $\tau = 0.5$ in imperfect synchronization case.

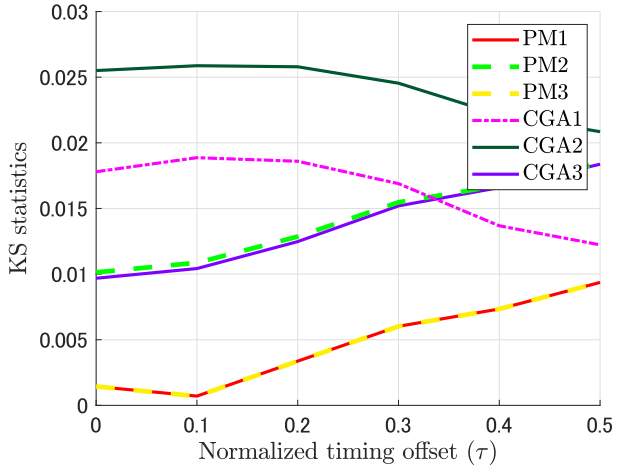

FIGURE 17. KS statistics as a function of τ with $\gamma = 0$dB, $M = 64$ and $K = 30$ in imperfect synchronization case.

of target P_D is plotted in the figure when $K = 30$, $\gamma = 0$ dB. The gap between the obtained P_D and target P_D under fading channel is smaller than the gap under AWGN channel, while PM1 and PM3 can achieve the best performance. The results in Figs. 12 and 13 indicate that the gap between PM3 (or PM1) and the conventional models in Fig. 15 would increase for smaller K or smaller γ.

C. AWGN CHANNEL WITH WITH IMPERFECT SYNCHRONIZATION

In this section, the simulation results here are only considered in $0 \leq \tau \leq 0.5$ because normalized timing offset τ is symmetric with respect to $\tau = 0$. For achieving $I(k) = 0$, not only perfect synchronization but also matched filter based approach with an appropriate filter, such as a square-root-raised-cosine filter, may be required. However, this is not practical. Therefore, this section assumes non-matched filter case: square-root-raised-cosine filter with the roll-off factor $\beta = 0.2$ as the transmitting filter and any filter with sufficiently wider bandwidth than that of the transmitting filter as the receiving filter. The imperfect synchronization and non-matched filter lead to non-zero ISI in (]]2).

Fig. 16 shows the PDFs of the proposed models and empirical PDFs with $M = 4, 16, 64, 256$, $\tau = 0.5$, and $\gamma = 0$ dB. Fig. 16 indicates that the proposed models can provide reasonably accurate PDFs even when there is sampling timing error.

Fig. 17 shows the KS statistics as a function of τ with $M = 64$, $K = 30$, $\gamma = 0$ dB. This numerical evaluation indicates that PM1 and PM3 are still more accurate than other models in any τ.

In a practical case, τ is not known at the ED and the design of ED under imperfect synchronization is one of the issues. For this issue, we design ED with a predetermined τ which is denoted by τ'. Specifically, the threshold is set based on

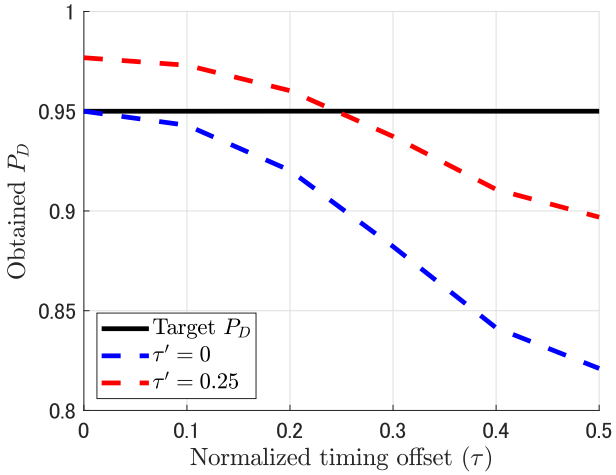

FIGURE 18. Obtained detection probability as a function of actual normalized timing offset τ with $\gamma = 0$ dB, $K = 30$ and assumed normalized timing offset $\tau' = 0$ and 0.25 in imperfect synchronization case.

the target P_D and the predetermined τ'. Fig. 18 shows the obtained detection probability as a function of actual normalized timing offset τ with the target $P_D = 0.95$, $M = 64$, $K = 30$, and $\gamma = 0$ dB. In this result, we evaluate the ED with $\tau' = 0$ and $\tau' = 0.25$. The result indicates that $\tau' \neq \tau$ leads to the error between the obtained P_D and the target $P_D = 0.95$. However, the maximum error can be relatively suppressed by $\tau' = 0.25$ compared to the case of $\tau' = 0$.

V. DISCUSSION

This section comprehensively discusses the performance of models shown in this paper. Table 1 summarizes the approximation types and the required computational cost.

Although ES can provide the actual distribution, the derivation of actual distribution of λ_A (15) requires significant computational cost as shown in Fig 1. In CGA1, CGA2, CGA3 and PM2, Gaussian approximation is used in either the distribution for signal component or the distribution for observed energy. These models can reduce the computational cost significantly compared to the cost in ES. In addition, the numerical evaluations reveal that CGA3 and PM2 in which the mean and variance are obtained by considering QAM signal can achieve relatively accurate PDF compared to CGA1 and CGA2. The difference between PM2 and CGA3 is whether they are independent of or dependent on M, respectively. Specifically, in the proposed models including PM2, M is set to ∞. Nevertheless, the numerical evaluations show that PM2 and CGA3 can achieve similarly accurate PDF.

Comparing PM1 and PM3, they can achieve the best accuracy among PMs and CGAs while PM3 can reduce computational cost compared to PM1 by avoiding K-fold convolution (22).

As confirmed in Figs. 3, 4, 11 and 16, the PMs can provide accurate PDF even though they approximate $M = \infty$. This is a preferred aspect of the PMs because they can handle adaptive modulation schemes where M can be changed dynamically according to the status of wireless communication channel, such as SNR. In the case of adaptive modulation scheme, the spectrum sensing based on ED has to perform without knowledge of M. For this matter, the PMs have an advantage because they are independent of M.

VI. CONCLUSION

In this paper, approximation models for the distribution of observed energy in case of M-ary QAM signals were investigated. In a previous work, an exact solution for the distribution was derived, however it requires significant computational costs. For this problem, we proposed three models based on an approximation to assume $M = \infty$ in the model for PDF of the observed energy. The first proposed model only employs the approximation of $M = \infty$ to derive the approximated PDF. In the second proposed model, Gaussian approximation for the observed energy is used and this can reduce the computational cost significantly. The third proposed model approximates the distribution of signal component by skew normal distribution and this can also reduce the computational cost compared to the first proposed model while it can achieve accurate distribution. In the comprehensive numerical evaluation, the proposed models and conventional models are evaluated and the results indicate that the third proposed model can achieve the most accurate distribution with a reasonable computational cost. In addition to AWGN channel case, more realistic cases are considered, i.e., Rayleigh fading channel and imperfect synchronization case. Numerical results indicate that the proposed models are still applicable to realistic cases. For future works, actual experiments are essential to confirm the validity of our proposed models.

APPENDIX A
DERIVATION OF $p_{\infty,1,A}(\lambda_A)$ FOR PM1

In the following, the derivation of $p_{\infty,1,A}(\lambda_A)$ is shown. Fig.2c is IQ plane, where the blue plane is aggregation of constellation points of $x[k]$ in $M = \infty$. Circumference l on the blue plane is expressed as follows:

$$l = \begin{cases} 2\pi r & (0 < r \leq a) \\ 4r\left(\frac{\pi}{2} - 2\cos^{-1}\frac{a}{r}\right) & (a \leq r \leq \sqrt{2}a), \end{cases} \tag{54}$$

where r is absolute value of amplitude and $2a$ is one side of IQ plane ($a = \sqrt{\frac{3}{2}}$), as Fig. 2c shows. Since l can be interpreted as likelihood of r, $p_{\infty,1,A}(r)$ is given by:

$$p_{\infty,1,A}(r) = \begin{cases} \frac{\pi r}{2a^2} & (0 < r \leq a) \\ \frac{r}{a^2}\left(\frac{\pi}{2} - 2\cos^{-1}\frac{a}{r}\right) & (a \leq r \leq \sqrt{2}a), \end{cases} \tag{55}$$

where $p_{\infty,1,A}(r)$ can be calculated by the normalization of $4a^2$, the area of IQ plane. Moreover, since λ_A is described as $2\gamma r^2$ when $K = 1$, $p_{\infty,1,A}(\lambda_A)$ can be calculated by using the transformation of random variable from r

TABLE 1. Summary of models shown in this paper based on computational cost and approximation.

Model	Type of approximation		Computational cost
	Signal component $x[k]$	Energy(λ_A or V')	
ES [29]	No approximation	No approximation	1 integration (13 or 39) & (15)
CGA1 [33]	Gaussian	No approximation	(18)
CGA2 [21]–[23]	Gaussian	$V' \sim$ Gaussian	(19)
CGA3 [30]	No approximation	$V' \sim$ Gaussian	(20)
PM1	$M = \infty$	No approximation	1 integration (13 or 39) K-fold convolution (22)
PM2	$M = \infty$	$V' \sim$ Gaussian	(27)
PM3	$M = \infty$	$\lambda_A \sim$ Skew normal	1 integration (13 or 39)

to λ_A as follows:

$$p_{\infty,1,A}(\lambda_A) = \begin{cases} \dfrac{\pi}{8\gamma a^2} & (0 < \lambda_A \le 2\gamma a^2) \\ \dfrac{\pi}{2} - 2\cos^{-1}\sqrt{\dfrac{2\gamma a^2}{\lambda_A}} & (2\gamma a^2 \le \lambda_A \le 4\gamma a^2). \end{cases} \quad (56)$$

APPENDIX B
PROOF OF THE EXPECTATION, VARIANCE AND SKEWNESS OF λ FOR PM2 AND PM3

This appendix shows the derivation of $\mu_{\lambda_A}, \sigma^2_{\lambda_A}$ and κ_{λ_A} based on (56). First of all, we consider the expectation, variance and skewness of λ_A when $K = 1$, denoted by $E_1[\lambda_A]$, $Var_1[\lambda_A]$ and $\kappa_1[\lambda_A]$, defined as

$$E_1[\lambda_A] = \int_{-\infty}^{\infty} \lambda_A p_{\infty,1,A}(\lambda_A) d\lambda_A, \quad (57)$$

$$Var_1[\lambda_A] = \int_{-\infty}^{\infty} (\lambda_A - E_1[\lambda_A])^2 p_{\infty,1,A}(\lambda_A) d\lambda_A, \quad (58)$$

$$\kappa_1[\lambda_A] = \int_{-\infty}^{\infty} \frac{(\lambda_A - E_1[\lambda_A])^3}{Var_1[\lambda_A]} p_{\infty,1,A}(\lambda_A) d\lambda_A, \quad (59)$$

where $p_{\infty,1,A}(\lambda_A)$ is PDF of λ_A when $M = \infty$ in (56). In the following, we calculate $E_1[\lambda_A]$ as follows:

$$\begin{aligned} E_1[\lambda_A] &= \int_0^{4\gamma a^2} \lambda_A \frac{\pi}{8\gamma a^2} d\lambda_A \\ &\quad - \frac{1}{2\gamma a^2} \int_{2\gamma a^2}^{4\gamma a^2} \lambda_A \cos^{-1}\sqrt{\frac{2\gamma a^2}{\lambda_A}} d\lambda_A \\ &= \pi\gamma a^2 - 4\gamma a^2 \int_1^{\sqrt{2}} x^3 \cos^{-1}\frac{1}{x} dx \\ &= \frac{4}{3}\gamma a^2 = 2\gamma \quad \left(\because a = \sqrt{\frac{3}{2}}\right), \end{aligned} \quad (60)$$

where $\cos^{-1}$ denotes arccosine function and x satisfies

$$x = \sqrt{\frac{\lambda_A}{2\gamma a^2}}. \quad (61)$$

Based on (60), we calculate $Var_1[\lambda_A]$ as follows:

$$\begin{aligned} Var_1[\lambda_A] &= \int_{-\infty}^{\infty} (\lambda_A - 2\gamma)^2 p_{\infty,1,A}(\lambda_A) d\lambda_A \\ &= \int_{-\infty}^{\infty} \lambda_A^2 p_{\infty,1,A}(\lambda_A) d\lambda_A \\ &\quad -4\gamma \int_{-\infty}^{\infty} \lambda_A p_{\infty,1,A}(\lambda_A) d\lambda_A \\ &\quad +4\gamma^2 \int_{-\infty}^{\infty} p_{\infty,1,A}(\lambda_A) d\lambda_A \\ &= \int_{-\infty}^{\infty} \lambda_A^2 p_{\infty,1,A}(\lambda_A) d\lambda_A - 4\gamma E_1[\lambda_A] + 4\gamma^2 \\ &= \int_{-\infty}^{\infty} \lambda_A^2 p_{\infty,1,A}(\lambda_A) d\lambda_A - 4\gamma^2. \end{aligned} \quad (62)$$

Here we calculate

$$\begin{aligned} &\int_{-\infty}^{\infty} \lambda_A^2 p_{\infty,1,A}(\lambda_A) d\lambda_A \\ &= \int_0^{4\gamma a^2} \lambda_A^2 \frac{\pi}{8\gamma a^2} d\lambda_A - \frac{1}{2\gamma a^2} \int_{2\gamma a^2}^{4\gamma a^2} \lambda_A^2 \cos^{-1}\sqrt{\frac{2\gamma a^2}{\lambda_A}} d\lambda_A \\ &= \frac{8}{3}\pi\gamma^2 a^4 - 8\gamma^2 a^4 \int_1^{\sqrt{2}} x^5 \cos^{-1}\frac{1}{x} dx \\ &= \frac{112}{45}\gamma^2 a^4 = \frac{28}{5}\gamma^2 \quad \left(\because a = \sqrt{\frac{3}{2}}\right), \end{aligned} \quad (63)$$

therefore,

$$\begin{aligned} Var_1[\lambda_A] &= \frac{28}{5}\gamma^2 - 4\gamma^2 \\ &= \frac{8}{5}\gamma^2. \end{aligned} \quad (64)$$

Based on (60) and (64), we calculate $\kappa_1[\lambda_A]$ as follows:

$$\begin{aligned} \kappa_1[\lambda_A] &= \int_{-\infty}^{\infty} \frac{(\lambda_A - E_1[\lambda_A])^3}{Var_1[\lambda_A]^{\frac{3}{2}}} p_{\infty,1,A}(\lambda_A) d\lambda_A \\ &= \frac{5\sqrt{5}}{16\sqrt{2}\gamma^3} \left\{ \int_{-\infty}^{\infty} \lambda_A^3 p_{\infty,1,A}(\lambda_A) d\lambda_A \right. \\ &\quad - 6\gamma \int_{-\infty}^{\infty} \lambda_A^2 p_{\infty,1,A}(\lambda_A) d\lambda_A \\ &\quad \left. + 12\gamma^2 \int_{-\infty}^{\infty} \lambda_A p_{\infty,1,A}(\lambda_A) d\lambda_A \right. \end{aligned}$$

$$- 8\gamma^3 \int_{-\infty}^{\infty} p_{\infty,1,A}(\lambda_A) d\lambda_A \Bigg\}$$
$$= \frac{5\sqrt{5}}{16\sqrt{2}\gamma^3} \left\{ \int_{-\infty}^{\infty} \lambda_A^3 p_{\infty,1,A}(\lambda_A) d\lambda_A - \frac{168}{5}\gamma^3 + 24\gamma^3 - 8\gamma^3 \right\}. \quad (65)$$

Here we calculate

$$\int_{-\infty}^{\infty} \lambda_A^3 p_{\infty,1,A}(\lambda_A) d\lambda_A$$
$$= \int_0^{4\gamma a^2} \lambda_A^3 \frac{\pi}{8\gamma a^2} d\lambda_A - \frac{1}{2\gamma a^2} \int_{2\gamma a^2}^{4\gamma a^2} \lambda_A^3 \cos^{-1} \sqrt{\frac{2\gamma a^2}{\lambda_A}} d\lambda_A$$
$$= 8\pi\gamma^3 a^6 - 16\gamma^3 a^6 \int_1^{\sqrt{2}} x^7 \cos^{-1} \frac{1}{x} dx$$
$$= \frac{192}{35}\gamma^3 a^6 = \frac{648}{35}\gamma^3 \quad \left(\because a = \sqrt{\frac{3}{2}} \right), \quad (66)$$

therefore,

$$\kappa_1[\lambda_A] = \frac{5\sqrt{5}}{16\sqrt{2}\gamma^3} \left\{ \frac{648}{35}\gamma^3 - \frac{168}{5}\gamma^3 + 24\gamma^3 - 8\gamma^3 \right\}$$
$$= \frac{\sqrt{10}}{7}. \quad (67)$$

Finally, because of linearity, μ_{λ_A} and $\sigma^2_{\lambda_A}$ can be expressed as follows:

$$\mu_{\lambda_A} = K \cdot E_1[\lambda_A] = 2K\gamma$$
$$\sigma^2_{\lambda_A} = K \cdot Var_1[\lambda_A] = \frac{8}{5}K\gamma^2$$
$$\kappa_{\lambda_A} = \frac{\kappa_1[\lambda_A]}{\sqrt{K}} = \frac{\sqrt{10}}{7\sqrt{K}}. \quad (68)$$

REFERENCES

[1] G. Staple and K. Werbach, "The end of spectrum scarcity [spectrum allocation and utilization]," *IEEE Spectr.*, vol. 41, no. 3, pp. 48–52, Mar. 2004.
[2] J. Reed, M. Vassiliou, and S. Shah, "The role of new technologies in solving the spectrum shortage [point of view]," *Proc. IEEE*, vol. 104, no. 6, pp. 1163–1168, Jun. 2016.
[3] Federal Communications Commission, "Spectrum policy task force report," FCC, Washington, DC, USA, Tech. Rep. Docket, nos. 02–135, Nov. 2002.
[4] I. F. Akyildiz, W.-Y. Lee, M. C. Vuran, and S. Mohanty, "NeXt generation/dynamic spectrum access/cognitive radio wireless networks: A survey," *Comput. Netw.*, vol. 50, pp. 2127–2159, Sep. 2006.
[5] W. S. H. M. W. Ahmad, N. A. M. Radzi, F. S. Samidi, A. Ismail, F. Abdullah, M. Z. Jamaludin, and M. N. Zakaria, "5G technology: Towards dynamic spectrum sharing using cognitive radio networks," *IEEE Access*, vol. 8, pp. 14460–14488, 2020.
[6] K. Umebayashi, S. Tiiro, and J. Lehtomäki, "Development of a measurement system for spectrum awareness," in *Proc. 1st Int. Conf. 5G Ubiquitous Connectivity*, 2014, pp. 234–239.
[7] T. Yucek and H. Arslan, "A survey of spectrum sensing algorithms for cognitive radio applications," *IEEE Commun. Surveys Tuts.*, vol. 11, no. 1, pp. 116–130, 1st Quart., 2009.
[8] Y. Arjoune and N. Kaabouch, "A comprehensive survey on spectrum sensing in cognitive radio networks: Recent advances, new challenges, and future research directions," *Sensors*, vol. 19, no. 1, p. 126, Jan. 2019.
[9] J. G. Proakis and M. Salehi, *Digital Communications*, 5th ed. New York, NY, USA: McGraw-Hill, 2007.
[10] Y. Arjoune, Z. E. Mrabet, H. E. Ghazi, and A. Tamtaoui, "Spectrum sensing: Enhanced energy detection technique based on noise measurement," in *Proc. IEEE 8th Annu. Comput. Commun. Workshop Conf. (CCWC)*, Jan. 2018, pp. 828–834.
[11] F. Salahdine, H. E. Ghazi, N. Kaabouch, and W. F. Fihri, "Matched filter detection with dynamic threshold for cognitive radio networks," in *Proc. Int. Conf. Wireless Netw. Mobile Commun. (WINCOM)*, Oct. 2015, pp. 1–6.
[12] A. Parvathy and G. Narayanan, "Comparative study of energy detection and matched filter based spectrum sensing techniques," in *Proc. 12th Int. Conf. Comput. Intell. Commun. Netw. (CICN)*, Sep. 2020, pp. 147–153.
[13] W. Wu, Z. Wang, L. Yuan, F. Zhou, F. Lang, B. Wang, and Q. Wu, "IRS-enhanced energy detection for spectrum sensing in cognitive radio networks," *IEEE Wireless Commun. Lett.*, vol. 10, no. 10, pp. 2254–2258, Oct. 2021.
[14] B. Soni, D. K. Patel, Z. Ding, Y. L. Guan, and S. Sun, "On sensing performance of multi-antenna mobile cognitive radio conditioned on primary user activity statistics," *IEEE Trans. Wireless Commun.*, vol. 21, no. 5, pp. 3381–3394, May 2022.
[15] H. Oh and H. Nam, "Energy detection scheme in the presence of burst signals," *IEEE Signal Process. Lett.*, vol. 26, no. 4, pp. 582–586, Apr. 2019.
[16] Y. Arjoune, Z. E. Mrabet, H. E. Ghazi, and A. Tamtaoui, "Spectrum sensing: Enhanced energy detection technique based on noise measurement," in *Proc. IEEE 8th Annu. Comput. Commun. Workshop Conf. (CCWC)*, Jan. 2018, pp. 828–834.
[17] S. Kay, *Fundamentals of Statistical Signal Processing: Detection Theory*. Upper Saddle River, NJ, USA: Prentice-Hall, 1998.
[18] H. Urkowitz, "Energy detection of unknown deterministic signals," *Proc. IEEE*, vol. 55, no. 4, pp. 523–531, Apr. 1967.
[19] F. F. Digham, M. S. Alouini, and M. K. Simon, "On the energy detection of unknown signals over fading channels," in *Proc. IEEE Int. Conf. Commun. (ICC)*, vol. 5, May 2003, pp. 3575–3579.
[20] L. Hanzo, M. Münster, B. Choi, and T. Keller, *OFDM and MC-CDMA for Broadband Multi-User Communications, WLANs and Broadcasting*. Hoboken, NJ, USA: Wiley, 2005.
[21] M. Lopez-Benitez and F. Casadevall, "Improved energy detection spectrum sensing for cognitive radio," *IET Commun.*, vol. 6, no. 8, pp. 785–796, May 2012.
[22] R. Umar, A. U. H Sheikh, and M. Deriche, "Unveiling the hidden assumptions of energy detector based spectrum sensing for cognitive radios," *IEEE Commun. Surveys Tuts.*, vol. 16, no. 2, pp. 713–728, 2nd Quart. 2014.
[23] Z. Ye, G. Memik, and J. Grosspietsch, "Energy detection using estimated noise variance for spectrum sensing in cognitive radio networks," in *Proc. IEEE Wireless Commun. Netw. Conf.*, Mar. 2008, pp. 711–716.
[24] G. Mahendru, A. Shukla, and P. Banerjee, "A novel mathematical model for energy detection based spectrum sensing in cognitive radio networks," *Wireless Pers. Commun.*, vol. 110, no. 3, pp. 1237–1249, Feb. 2020.
[25] *IEEE Standard for High Data Rate Wireless Multi-Media Networks–Amendment 2: 100 Gb/s Wireless Switched Point-Topoint Physical Layer*, Standard 802.15.3d-2017 (Amendment to IEEE Std 802.15.3-2016 as Amended by IEEE Std 802.15.3e- 2017), 2017, pp. 1–55.
[26] T. Harter, "Generalized Kramers–Kronig receiver for coherent terahertz communications," *Nature Photon.*, vol. 14, no. 10, pp. 601–606, 2020.
[27] D. Pirrone, A. Ferraro, D. C. Zografopoulos, W. Fuscaldo, P. Szriftgiser, G. Ducournau, and R. Beccherelli, "Metasurface-based filters for high data rate THz wireless communication: Experimental validation of a 14 Gbps OOK and 104 Gbps QAM-16 wireless link in the 300 GHz band," *IEEE Trans. Wireless Commun.*, vol. 21, no. 10, pp. 8688–8697, Oct. 2022.
[28] I. Dan, G. Ducournau, S. Hisatake, P. Szriftgiser, R.-P. Braun, and I. Kallfass, "A terahertz wireless communication link using a superheterodyne approach," *IEEE Trans. THz Sci. Technol.*, vol. 10, no. 1, pp. 32–43, Jan. 2020.
[29] D. S. Chaves and A. N. Barreto, "Energy detection spectrum sensing of M-ary QAM systems over AWGN channels," in *Proc. Int. Symp. Wireless Commun. Syst. (ISWCS)*, Aug. 2012, pp. 106–110.
[30] S. Tariq, "Analysis of joint multiband sensing-time M-QAM signal detection in cognitive radios," *ETRI J.*, vol. 34, no. 6, pp. 892–899, Dec. 2012.
[31] S. Ishihara, K. Umebayashi, and J. Lehtomaki, "Energy detection for M-QAM signals," in *Proc. IEEE 93rd Veh. Technol. Conf. (VTC-Spring)*, Apr. 2021, pp. 1–5.
[32] X. Qiu and K. Chawla, "On the performance of adaptive modulation in cellular systems," *IEEE Trans. Commun.*, vol. 47, no. 6, pp. 884–895, Jun. 1999.
[33] J. Ma, G. Zhao, and Y. Li, "Soft combination and detection for cooperative spectrum sensing in cognitive radio networks," *IEEE Trans. Wireless Commun.*, vol. 7, no. 11, pp. 4502–4507, Nov. 2008.
[34] A. H. Nuttall, "Some integrals involving the Q_M function (Corresp.)," *IEEE Trans. Inf. Theory*, vol. IT-21, no. 1, pp. 95–96, Jan. 1975.

[35] J. Ma, G. Y. Li, and B. H. Juang, "Signal processing in cognitive radio," *Proc. IEEE*, vol. 97, no. 5, pp. 805–823, May 2009.
[36] H. Nussbaumer, *Fast Fourier Transf. Convolution Algorithms* (Springer Series in Information Sciences). Berlin, Germany: Springer, 2012.
[37] M. A. Carlton and J. L. Devore, *Probability With Applications in Engineering, Science, and Technology*. Cham, Switzerland: Springer, 2017.
[38] A. Azzalini, "The skew-normal distribution and related multivariate families," *Scandin. J. Statist.*, vol. 32, no. 2, pp. 159–188, 2005.
[39] V. I. Kostylev, "Energy detection of a signal with random amplitude," in *Proc. IEEE Int. Conf. Commun. Conf.*, vol. 3, Apr. 2002, pp. 1606–1610.
[40] P. Zhang, R. Qiu, and N. Guo, "Demonstration of spectrum sensing with blindly learned features," *IEEE Commun. Lett.*, vol. 15, no. 5, pp. 548–550, May 2011.
[41] D. Cabric, A. Tkachenko, and R. Brodersen, "Spectrum sensing measurements of pilot, energy, and collaborative detection," in *Proc. MILCOM*, Oct. 2006, pp. 1–7.
[42] K. Kim, Y. Xin, and S. Rangarajan, "Energy detection based spectrum sensing for cognitive radio: An experimental study," in *Proc. IEEE Global Telecommun. Conf. GLOBECOM*, Dec. 2010, pp. 1–5.
[43] N. Smirnov, "Table for estimating the goodness of fit of empirical distributions," *Ann. Math. Statist.*, vol. 19, no. 2, pp. 279–281, Jun. 1948.
[44] M. López-Benítez and F. Casadevall, "Time-dimension models of spectrum usage for the analysis, design, and simulation of cognitive radio networks," *IEEE Trans. Veh. Technol.*, vol. 62, no. 5, pp. 2091–2104, Jun. 2013.
[45] Y. Norouzi, F. Gini, M. M. Nayebi, and M. Greco, "Non-coherent radar CFAR detection based on goodness-of-fit tests," *IET Radar, Sonar Navigat.*, vol. 1, no. 2, pp. 98–105, Apr. 2007.
[46] J. Lehtomaki, J. Vartiainen, M. Juntti, and H. Saarnisaari, "Spectrum sensingwith forward methods," in *Proc. MILCOM*, Oct. 2006, pp. 1–7.
[47] G. Caso, L. D. Nardis, G. C. Ferrante, and M.-G. D. Benedetto, "Cooperative spectrum sensing based on majority decision under CFAR and CDR constraints," in *Proc. IEEE 24th Int. Symp. Pers., Indoor Mobile Radio Commun. (PIMRC Workshops)*, Sep. 2013, pp. 51–55.
[48] M. Lopez-Benitez, F. Casadevall, and C. Martella, "Performance of spectrum sensing for cognitive radio based on field measurements of various radio technologies," in *Proc. Eur. Wireless Conf. (EW)*, Apr. 2010, pp. 969–977.

SHUN ISHIHARA received the B.E. degree from the Tokyo University of Agriculture and Technology, in 2021, where he is currently pursuing the M.E. degree. His research interests include array antenna and energy detection.

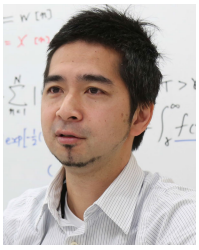

KENTA UMEBAYASHI (Member, IEEE) received the LL.B. degree from Ritsumeikan University, Japan, in 1996, and the B.E., M.E., and Ph.D. degrees from Yokohama National University, Japan, in 1999, 2001, and 2004, respectively. From 2004 to 2006, he was a Research Scientist with the Centre for Wireless Communications, University of Oulu, Finland. He is currently a Professor with the Tokyo University of Agriculture and Technology, Japan. He was a Principal Investigator of four grants-in-aid for scientific research projects and three strategic information and communications research and development promotion programme projects. His research interests include the areas of signal detection and estimation theories for wireless communication, signal processing for multiple antenna systems, cognitive radio networks, and terahertz band wireless communications. He received the Best Paper Award at the 2012 IEEE WCNC and the Best Paper Award at the 2015 IEEE WCNC Workshop from IWSS.

JANNE J. LEHTOMÄKI (Member, IEEE) received the Doctorate degree from the University of Oulu, Finland, in 2005. Currently, he is an Adjunct Professor at the Centre for Wireless Communications, University of Oulu. In Fall 2013, he spent the semester at Georgia Tech, Atlanta, USA, as a Visiting Scholar. He is also focusing on spectrum measurements and terahertz band wireless communications. He is also an Editorial Board Member of *Physical Communication*. He has coauthored the paper receiving the Best Paper Award in IEEE WCNC 2012. He was the General Co-Chair of IEEE WCNC 2017 International Workshop on Smart Spectrum, the TPC Co-Chair for IEEE WCNC 2015 and 2016 International Workshop on Smart Spectrum, and the Publicity/Publications Co-Chair for ACM NANOCOM 2015, 2016, and 2017. He has served as a Guest Associate Editor for the *IEICE Transactions on Communications* Special Section (February 2014 and July 2017) and as a Managing Guest Editor for *Nano Communication Networks* Special Issue (June 2016).